Adult enteric nervous system in health is maintained by a dynamic balance between neuronal apoptosis and neurogenesis

Subhash Kulkarni[a], Maria-Adelaide Micci[b], Jenna Leser[a], Changsik Shin[c], Shiue-Cheng Tang[d], Ya-Yuan Fu[a], Liansheng Liu[a], Qian Li[a], Monalee Saha[a], Cuiping Li[a], Grigori Enikolopov[e,f], Laren Becker[g], Nikolai Rakhilin[h,i], Michael Anderson[j,k,l,m], Xiling Shen[h,i], Xinzhong Dong[j,k,l,m], Manish J. Butte[n], Hongjun Song[j,o], E. Michelle Southard-Smith[p], Raj P. Kapur[q], Milena Bogunovic[c], and Pankaj J. Pasricha[a,1]

[a]Center for Neurogastroenterology, Department of Medicine, The Johns Hopkins University School of Medicine, Baltimore, MD 21205; [b]Department of Anesthesiology, University of Texas Medical Branch, Galveston, TX 77555; [c]Department of Microbiology and Immunology, College of Medicine, Pennsylvania State University, Hershey, PA 17033; [d]National Tsing Hua University, Hsinchu 300, Taiwan; [e]Cold Spring Harbor Laboratory, Cold Spring Harbor, NY 11724; [f]Center for Developmental Genetics, Department of Anesthesiology, Stony Brook University, Stony Brook, NY 11794; [g]Division of Gastroenterology, Stanford University School of Medicine, Stanford, CA 94305; [h]Department of Biomedical Engineering, Duke University, Durham, NC 27708; [i]School of Electrical and Computer Engineering, Cornell University, Ithaca, NY 14853; [j]Solomon H. Snyder Department of Neuroscience, The Johns Hopkins University School of Medicine, Baltimore, MD 21205; [k]Department of Neurosurgery, The Johns Hopkins University School of Medicine, Baltimore, MD 21205; [l]Department of Dermatology, Center for Sensory Biology, The Johns Hopkins University, School of Medicine, Baltimore, MD 21205; [m]Howard Hughes Medical Institute, The Johns Hopkins University, School of Medicine, Baltimore, MD 21205; [n]Department of Pediatrics, David Geffen School of Medicine, University of California, Los Angeles, CA 90095; [o]Institute for Cellular Engineering, Department of Neurology, The Johns Hopkins University, School of Medicine, Baltimore, MD 21205; [p]Division of Genetic Medicine, Vanderbilt University Medical Center, Nashville, TN 37232; and [q]Department of Laboratories, Seattle Children's Hospital, Seattle, WA 98105

Edited by Solomon H. Snyder, The Johns Hopkins University School of Medicine, Baltimore, MD, and approved March 24, 2017 (received for review November 28, 2016)

According to current dogma, there is little or no ongoing neurogenesis in the fully developed adult enteric nervous system. This lack of neurogenesis leaves unanswered the question of how enteric neuronal populations are maintained in adult guts, given previous reports of ongoing neuronal death. Here, we confirm that despite ongoing neuronal cell loss because of apoptosis in the myenteric ganglia of the adult small intestine, total myenteric neuronal numbers remain constant. This observed neuronal homeostasis is maintained by new neurons formed in vivo from dividing precursor cells that are located within myenteric ganglia and express both Nestin and p75NTR, but not the pan-glial marker Sox10. Mutation of the phosphatase and tensin homolog gene in this pool of adult precursors leads to an increase in enteric neuronal number, resulting in ganglioneuromatosis, modeling the corresponding disorder in humans. Taken together, our results show significant turnover and neurogenesis of adult enteric neurons and provide a paradigm for understanding the enteric nervous system in health and disease.

enteric neurons | adult neurogenesis | Nestin | enteric neural precursor cells | neuronal apoptosis

The enteric nervous system (ENS) controls or regulates vital gastrointestinal functions, including motility, secretion, local immunity, and inflammation, and represents the largest collection of autonomous neurons outside of the brain (1). Disorders involving the ENS are common and major contributors to the health burden throughout the world (2). Although the ENS is constantly exposed to mechanical stress (3), as well as potential environmental threats from luminal contents (4), it is not known how the numbers of enteric neurons in the healthy adult small intestine remain remarkably constant for most of adult life (5). Although continuous production of new neurons in the gut would appear to be needed to offset the observed apoptosis-mediated neuronal loss (6), such neurogenesis has been remarkably difficult to demonstrate and in vivo enteric neurogenesis in adults remains highly controversial (7–10). A second and related conundrum in this field has been the inability to confidently determine if a true enteric neural precursor cell (ENPC) exists in the gut, despite ample demonstration of stem-cell like behavior (self-renewal and multipotency) in vitro of cells isolated from embryonic and adult intestine using a variety of markers (7–9, 11–23). In this study, we have resolved these controversies by successfully identifying the ENPC capable of rapid neurogenesis in vivo to keep up with what we show to be a high rate of ongoing neuronal apoptosis in the adult small intestine. Furthermore, unchecked proliferation of these precursor cells leads to an intestinal phenotype that resembles human ganglioneuromatosis, a disorder of intestinal dysmotility seen in patients (24). Our results indicate a remarkable rate of turnover of adult neurons in the small intestine and provide a unique paradigm for understanding the ENS in health and disease.

Results

Significant Neuronal Loss Occurs in the ENS in the Healthy Adult Gut. We determined if enteric neurons are dying at a significant rate in healthy adults, thus establishing the need for replacement by neurogenesis. First, we stained adult murine myenteric ganglia with a cleaved caspase-3–specific antibody that has previously been shown to mark neurons from the central and ENS that are fated for apoptosis (25, 26). We found that a significant

Significance

The demonstration of a robust neurogenesis program in the adult gut and the existence of an enteric neural precursor cell (ENPC) responsible for the same has profound biological and clinical implications. This demonstrates the presence of robust adult neurogenesis outside of the CNS, and indicates the vulnerability of the enteric nervous system to exogenous influences, even in adults. As an example, it is possible that acquired diseases of the enteric nervous system, such as achalasia, may result from a loss of ENPC, analogous to congenital disorders, such as Hirschsprung's. The ability to identify the adult ENPC will therefore enable a new understanding of the pathogenesis of enteric neuromuscular diseases as well as the development of novel regenerative therapies.

Author contributions: S.K., M.-A.M., H.S., M.B., and P.J.P. designed research; S.K., J.L., C.S., S.-C.T., Y.-Y.F., L.L., Q.L., M.S., C.L., L.B., N.R., M.A., M.B., and P.J.P. performed research; S.K., C.S., S.-C.T., M.S., G.E., N.R., M.A., X.S., X.D., M.J.B., E.M.S.-S., and P.J.P. contributed new reagents/analytic tools; S.K., M.-A.M., J.L., C.S., R.P.K., M.B., and P.J.P. analyzed data; and S.K., M.-A.M., and P.J.P. wrote the paper.

The authors declare no conflict of interest.

This article is a PNAS Direct Submission.

[1]To whom correspondence should be addressed. Email: ppasric1@jhmi.edu.

This article contains supporting information online at www.pnas.org/lookup/suppl/doi:10.1073/pnas.1619406114/-/DCSupplemental.

number (mean ± SE of percent cleaved caspase-3$^+$ neurons per ganglia = 11.49 ± 0.50, total numbers of ganglia counted = 48, from 3 adult mice) of myenteric neurons express the enzyme cleaved caspase-3 (Fig. 1*A*). The presence of significant levels of apoptotic neurons by this method in the young adult myenteric plexus was recently confirmed in an independent publication (27). Biochemical proof of the enzymatic activity of caspase-3 was then obtained using a fluorescently labeled caspase-3/7 substrate (Fig. 1*C*) (28), accompanied by in vivo labeling of myenteric neurons with propidium iodide (PI), which is indicative of dying cells (Fig. 1*B* and Fig. S1 *A* and *B*) (29–31).

Further proof of the limited longevity of adult enteric neurons was obtained using a nitric oxide synthase 1 (NOS1)-creER^{T2} mouse, which we have previously reported (32). This mouse was bred with a mouse containing a floxed tdTomato gene and the resulting NOS1-creER^{T2}:tdTomato progeny were administered tamoxifen (for 4 consecutive days) when adults. In mice that were killed immediately after induction (day 0), almost all NOS1-expressing neurons were labeled with tdTomato expression (Fig. 2*A*). However, in mice that were killed 7 d after the tamoxifen treatment, we observed the emergence of a population of NOS1-expressing neurons that were not labeled with tdTomato (Fig. 2*B*), suggesting that these NOS1-expressing neurons were newly born. This observed loss of tdTomato-labeled nitrergic (NOS1$^+$) neurons was corroborated using our previously described technique of in vivo imaging (32). On imaging the same myenteric region of live NOS1-creER^{T2}:tdTomato mice that were induced as before with tamoxifen, we observed a loss of labeled neurons within a 24-h period, accompanied by robust remodeling of neural networks (Fig. 2*C*). However, even with the observed loss of nitrergic neurons over the course of 7 d, the total number of neurons within myenteric ganglia was conserved (Fig. 2*F*) (mean numbers ± SE of HuC/D$^+$ neurons per myenteric ganglia: 20.52 ± 1.58 vs. 19.33 ± 2.36 at day 0 and day 7, respectively). On the other hand, nearly a third (~31%) of preexisting NOS1 neurons labeled with tdTomato were lost at day 7 (Fig. 2*F*) (mean numbers ± SE of tdTomato$^+$ neurons per

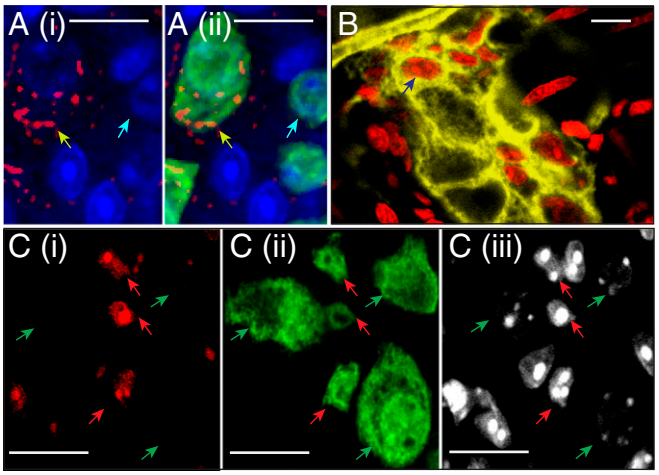

Fig. 1. Adult myenteric neurons undergo apoptosis-mediated cell death. (*A*, *i*) Cells within the myenteric ganglia that express the apoptosis marker cleaved caspase-3 (red) that (*ii*) also express HuC/D (green) represent apoptotic neurons (yellow arrow) compared with other myenteric neurons do not express cleaved caspase-3 (blue arrow). Nuclei are labeled with DAPI (blue). (*B*) Nuclei labeled in vivo with PI (red) within the myenteric ganglia of a ChAT-cre:YFP adult mouse, where cholinergic neurons are labeled with YFP (yellow), represent neurons with leaky cell membranes indicating apoptotic cells (dark-blue arrow). (*C*) Image of a myenteric ganglia of an adult C57BL/6 mouse, where apoptotic cells were labeled with (*i*) CellEvent caspase-3/7 detection dye (red) and then stained with (*ii*) HuC/D (green), shows the presence of a population of myenteric neurons that are positive (red arrows), as well as those negative for apoptotic markers (green arrows). (*iii*) DAPI labeled nuclei (light gray). (Scale bars, 10 μm.)

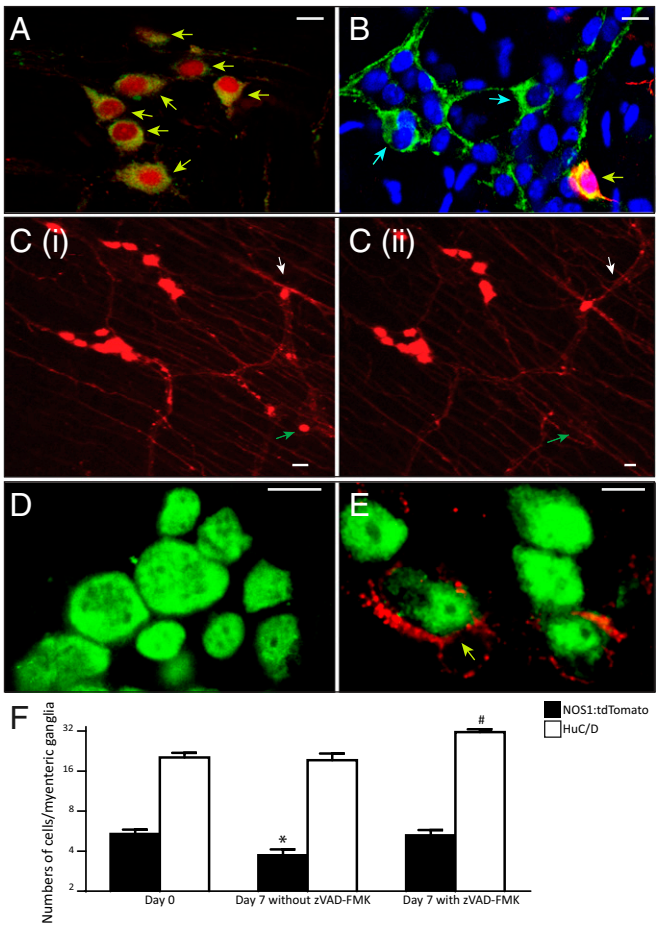

Fig. 2. Loss of myenteric neurons because of apoptosis can be quantified and can be arrested using an antiapoptotic drug. (*A* and *B*) Images of myenteric ganglia from an adult NOS1-creER^{T2}:tdTomato mouse that was killed the day after the cessation of tamoxifen induction (day 0) and stained with antisera against NOS1 (green) (*A*) and another that was killed 7 d after the cessation of tamoxifen induction (*B*). At day 0 (*A*), all NOS1-expressing neurons express tdTomato (yellow arrows), whereas at day 7 (*B*), a population of NOS1-expressing neurons that do not express tdTomato emerges (blue arrows). Nuclei are labeled in *B* with DAPI (blue). (Scale bars, 10 μm.) (*C*) A 2D projection of 3D images captured using live animal two-photon microscopy [(*i*) time 0 and (*ii*) time 24 h] from the same region of the myenteric plexus of NOS1-creER^{T2}:tdTomato mouse that was induced with tamoxifen before the imaging shows the disappearance of a tdTomato$^+$ nitrergic neuron (green arrow) within 24 h. The image also shows (white arrow) the appearance of new projections from a tdTomato$^+$ neuron that rapidly extend to form new network connections within 24 h, showing the robust plasticity of neuronal networks in the myenteric ganglia. (Scale bars, 10 μm.) (*D* and *E*) Representative images from myenteric ganglia that were stained with antisera against HuC/D (green) and antibody against cleaved caspase-3 (red) shows a lack of cleaved caspase-3 immunoreactivity in mice that were given the pan-caspase inhibitor zVAD-FMK (*E*), whereas mice that were not given the drug shows the presence of cleaved caspase-3–labeled myenteric neurons (yellow arrow in *E*). (Scale bars, 10 μm.) (*F*) Quantification of numbers of tdTomato$^+$ and HuC/D expressing neurons within myenteric ganglia from three different cohorts of mice killed at day 7 shows a significant reduction (*$P < 0.05$) in the numbers of tdTomato$^+$ neurons per ganglia in mice without zVAD-FMK compared with either day 0 or those given zVAD-FMK. The data also shows that total numbers of HuC/D$^+$ neurons within myenteric ganglia remain conserved between days 0 and 7 (without zVAD-FMK) although the numbers of tdTomato$^+$ neurons dwindle. Furthermore, an attenuation of apoptosis brought about by zVAD-FMK administration results in a concomitant significant increase in total numbers of myenteric neurons per ganglia ($^{\#}P < 0.05$) compared with the other two groups.

myenteric ganglia were reduced by ~31% at day 7: 3.70 ± 0.38; compared with mice at day 0: 5.31 ± 0.42, $P = 0.003$).

To determine whether the observed loss of mature tdTomato$^+$ neurons was because of apoptosis, we repeated the above experiment in another cohort of NOS1-creER^{T2}:tdTomato mice, this time treated with the pan-caspase inhibitor zVAD-FMK for 7 d, which suppressed the formation of cleaved caspase-3 within the adult myenteric ganglia (Fig. 2 *D* and *E*). Furthermore, in NOS1-creER^{T2}:tdTomato mice induced with tamoxifen as before, this treatment significantly attenuated the previously noted loss of tdTomato-labeled nitrergic neurons (Fig. 2*F*) (mean numbers ± SE of tdTomato$^+$ neurons per myenteric ganglia in pan-caspase inhibitor treated mice at day 7 posttamoxifen: 5.20 ± 0.50). As predicted, this arrest in death of nitrergic neurons also resulted in a significant increase in the global numbers of neurons (as measured by HuC/D$^+$ expression) (Fig. 2*F*) (mean numbers ± SE of HuC/D$^+$ neurons in a ganglia: 31.39 ± 1.57 vs. 19.33 ± 2.36 at day 7 posttamoxifen with and without zVAD-FMK, respectively; $P = 0.004$).

Myenteric Neurons Are Continuously Phagocytosed by Muscularis Macrophages in the Healthy Gut. We asked how dying neurons or neuronal debris resulting from this high rate of neuronal death are cleared away from the myenteric ganglia. Such a high rate of neuronal death necessitates an equally efficient method of clearance by phagocytic cells. A specialized subset of intestinal macrophages, known as muscularis macrophages, are anatomically and functionally associated with the myenteric plexus (33, 34). Because macrophages do not express the gene for choline acetyltransferase (ChAT) (35, 36), which is expressed by a large number of myenteric neurons (35), we used the ChAT-cre:tdTomato mouse to observe the phagocytosis of myenteric neurons by muscularis macrophages. On imaging the myenteric plexus of these mice when stained with antibodies against macrophages, we observed that cell bodies of tdTomato-expressing cholinergic neurons were engulfed by muscularis macrophages in both the small intestine and the colon (Fig. 3, Fig. S1 *C* and *D*, and Movie S1). Although we were able to observe engulfment of neurons by these macrophages through microscopy, we also studied the presence of tdTomato inclusions in intestinal macrophages using flow cytometry and found that although the mucosal and submucosal macrophages that are less associated with enteric neurons (33) showed a very small population of tdTomato-containing macrophages, significant numbers (~7.5%) of myenteric plexus-associated muscularis macrophages contained tdTomato in both small and large bowel, further supporting our imaging data (Fig. S1 *E* and *F*). Taking these data together, we observed that ENS-associated muscularis macrophages participate in phagocytosis of dying neurons and the active clearance of neuronal debris, and that this process is common for the both the small and large bowel.

Nestin Marks Putative ENPCs. Together, the above-mentioned results on conservation of total neuronal numbers, despite significant ongoing neuronal loss, provide robust evidence of significant neuronal turnover in healthy tissue, thereby indicating an active pool of ENPC. We next identified such cells using Nestin, a cytoskeletal protein (37) that is expressed by a variety of neural stem cells (38–42). tdTomato$^+$ neurospheres derived from the longitudinal muscle-myenteric plexus (LM-MP) layer of small intestines from tamoxifen-induced Nestin-creER^{T2}:tdTomato mice (where tdTomato expression in the myenteric plexus correlated with Nestin expression, Fig. S2*A*) differentiated into neurons in vitro and expressed neuronal NOS1, an enzyme characteristically expressed by inhibitory enteric neurons (Fig. 4*A*). Furthermore, cells from these tdTomato$^+$ neurospheres, when transplanted into the wall of adult mice, successfully engrafted and differentiated into HuC/D-labeled neurons in the myenteric ganglia of the host mice (Fig. 4*B* and Fig. S3*A*).

Anatomical Location of ENPC in the Adult Intestine. Having proven that Nestin is a suitable marker for ENPC, we then proceeded to determine the location of putative ENPC in vivo using a Nestin-GFP transgenic reporter mouse that one of our laboratories has previously described (39). Using previously described techniques

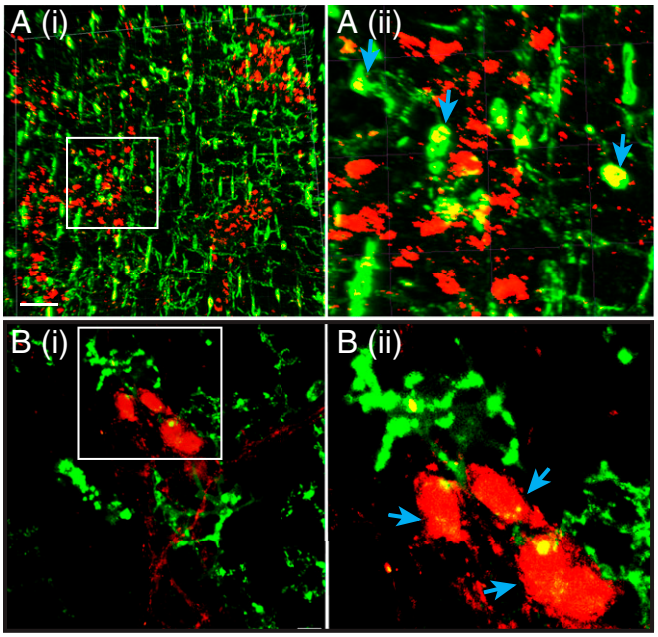

Fig. 3. Muscularis macrophages phagocytose myenteric neurons in healthy guts. (*A*, *i*) Two-photon microscopy of myenteric plexus from the colon of a ChAT-cre:tdTomato mouse shows tdTomato-expressing (red) cholinergic neurons along with MHC class II-labeled muscularis macrophages (green) shows an abundance of macrophages associated with the myenteric plexus. *Inset* (*i*) is magnified and shows (*ii*) the engulfment of tdTomato-expressing neuronal soma (red) in MHC II labeled macrophages (green; cyan arrows). (Scale bar, 50 μm.) (*B*, *i*) A 2D projection image of a *z*-stack of confocal microscopy images of neurons within the small intestinal myenteric ganglia shows the colocalization of ChAT-cre:tdTomato (red) signal along with that of CD11b-stained (green) muscularis macrophages. *Inset* (*i*) is magnified and shows (*ii*) the engulfment of tdTomato-expressing neuronal soma (red) by CD11b-stained macrophages (green; cyan arrows), suggesting phagocytosis of myenteric neurons by macrophages. (Scale bar, 10 μm.)

for optical clarification-aided microscopy of intestinal tissue (43), Nestin-GFP$^+$ cells in these mice form an extensive network of cells (Fig. 5 *A* and *B* and Movie S2) spanning most of the entire wall of the small intestine. They are particularly prominent in the submucosal zone and in the muscular layers, but are not present in the epithelial lining. Although, much of this network is perivascular in nature (Fig. 5*B*), a smaller collection of cells is present in the myenteric plexus (Fig. 5 *A* and *B* and Movies S2 and S3). Because enteric neurons and their precursors are derived from the neural crest (44, 45), we used a triple transgenic mouse (Wnt1-cre:tdTomato)-(Nestin-GFP) to establish the origin of Nestin-GFP$^+$ cells. Perivascular Nestin-GFP$^+$ cells are not labeled with tdTomato (Fig. 5*C*; unmerged images in Fig. S4*A*), and hence do not qualify as neural crest-derived precursors. Instead, they express NG2 (Fig. S4*B*), a characteristic marker of intestinal pericytes derived from serosal mesothelium (46). In contrast, Nestin-GFP$^+$ cells in the myenteric plexus are labeled with Wnt1-cre:tdTomato, indicating their origin from the neural crest. The intraganglionic Nestin-GFP$^+$ cells do not express the pan-neuronal marker PGP9.5 (Fig. 5*D*) and instead surround neuronal cell bodies (Fig. S5*C* and Movie S3). However, they express the low-affinity nerve growth factor receptor, p75NTR (Fig. 5*E*; unmerged images in Fig. S4*D*), CD49b (Fig. 5*F*; unmerged images in Fig. S4*C*), and the glial marker, S100β (Fig. S5*C*), both of which are known to mark cells that give rise to enteric neurons and glia or neurospheres in vitro (7, 8, 13). In contrast, perivascular Nestin-GFP$^+$ cells do not express p75NTR. Finally, Nestin$^+$ cells express the mitotic marker Ki67 at steady state (Fig. 5*G*; unmerged images in Fig. S4*G*) (mean ± SE numbers of myenteric ganglia with Nestin-GFP$^+$ cells

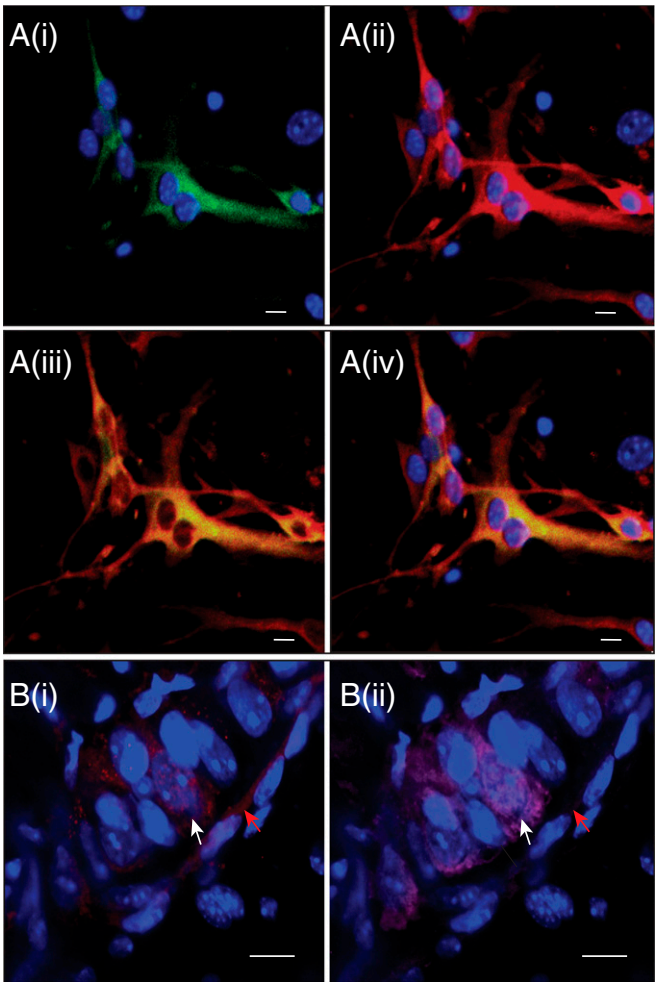

Fig. 4. Nestin marks putative enteric neuronal precursor cells in the adult gut wall. (*A*) In vitro cultured neurosphere-derived neurons from a Nestin-creER^{T2}:tdTomato mouse that (*i*) are stained with NOS1 (green) and (*ii*) express tdTomato (red) under Nestin-creER^{T2}induction, (*iii*) show colocalization providing evidence that Nestin-expressing cells generate neurospheres in culture that can be differentiated into nitrergic neurons; (*iv*) nuclei are stained with DAPI (blue). (Scale bars, 10 μm.) (*B*) Myenteric ganglia of an adult mouse where Nestin-creER^{T2}:tdTomato-derived neurosphere-derived cells were transplanted where (*i*) tdTomato^{+} graft derived cells (red; white arrow) (*ii*) form mature neurons that express HuC/D (magenta; white arrow), showing that graft-derived cells give rise to neurons. Additional tdTomato-expression can be noticed (red arrow) which does not show corresponding HuC/D colocalization. HuC/D and tdTomato channels separated in Fig. S3*A*. Nuclei are counterstained with DAPI (blue). (Scale bars, 10 μm.)

that coexpress Ki67: 0.44 ± 0.14), suggesting that these cells are actively proliferating.

Myenteric Nestin^{+}/p75NTR^{+} Express Stem Cell Behavior in Vitro. Having established the location of these putative ENPC, we next obtained definitive proof of their stem cell-like behavior using in vitro clonal assays in a defined culture medium (12, 40). By establishing the flow gates for p75NTR-expressing cells (Fig. 6*A*), we confirmed the coexpression of p75NTR in a subset of Nestin-GFP^{+} cells using FACS analysis (Fig. 6*B* and Fig. S2*B*). In vitro clonal analyses on all isolated myenteric cell populations showed that only Nestin-GFP^{+} cells proliferated (Fig. 6*C*) (mean ± SE of percentage of neurosphere-forming Nestin-GFP^{+} cells: 3.6 ± 0.4). Using similar clonal analysis on Nestin-GFP^{+} cells stained for p75NTR, we found that only cells labeled for both Nestin-GFP^{+} and p75NTR^{+} formed neurospheres (Fig. 6*D*). This population shows significant enrichment in the numbers of neurosphere-forming cells over its parent population of all Nestin-GFP^{+} cells (mean ± SE of percentage of neurosphere-forming proliferative cells when sorted for Nestin-GFP and p75NTR: 10.1 ± 0.5; $P <$ 0.01). Furthermore, these single cell-derived neurospheres produced both neurons and glia in differentiating conditions (Fig. 6*E*; unmerged monochrome images in Fig. S4*K*) (mean ± SE of percentage of neurospheres that differentiate to form both neurons and glia: 78.26 ± 4.35; only neurons: 0 ± 0; only glia: 2.22 ± 1.96).

Myenteric Nestin^{+} Cells Are Responsible for Neurogenesis in Vivo. Having shown their potential as precursors in vitro, we then tested whether myenteric Nestin-expressing cells are capable of neurogenesis in vivo in healthy adult gut using inducible Cre transgenic mice for fate-mapping experiments. Twelve hours after tamoxifen induction, adult Nestin-creER^{T2}:tdTomato mice did not show any expression of tdTomato in existing HuC/D^{+} neurons (Fig. 7*A*). However, 6 d after tamoxifen induction, adult myenteric neurons were labeled with tdTomato, proving their derivation from Nestin-expressing cells (Fig. 7*B*; unmerged images in Fig. S4*H*). To further quantify this phenomenon, we killed a cohort of mice 12 h, 24 h, 6 d, and 14 d after tamoxifen injection and found an increase in the proportion of tdTomato^{+} neurons in myenteric ganglia with time (Fig. 7*C*) (mean ± SE of mean percent of tdTomato^{+} neurons/ganglia: 12 h: 0.0 ± 0.0; 24 h: 0.20 ± 0.20; 6 d: 3.62 ± 2.54; and 14 d: 6.87 ± 1.89, $P < 0.05$). Some Nestin-derived cells in the myenteric ganglia also expressed S100β, showing that these precursors can generate asymmetrical progenies (Fig. S4 *E* and *F*).

New Neurons Arise from Precursors That Undergo Proliferation and Cell Division. Given that Nestin^{+} cells proliferate in vivo (Figs. 5*G* and 7*D*, and Fig. S5 *A* and *B*), we hypothesized that they can give rise to new neurons in a classic stem cell paradigm where the precursor cell divides to form a daughter cell that then differentiates into a neuron, rather than by direct transdifferentiation without an intermediate cell division. We therefore determined if mature neurons were derived from proliferating cells, which would indicate the former process. Under resting conditions, a stem cell divides asymmetrically to produce a precursor cell and another stem cell. The former goes on to differentiate into a mature cell, whereas the latter reenters the cell-cycle after a period. Hence, by using temporally spaced proliferation markers, both the original stem cell and its daughter stem cell can be labeled and their fate followed in vivo.

We first optimized experimental protocols to detect thymidine analogs by using a variety of denaturation protocols (47) and then tweaking them for sectioned and whole-mount intestinal tissue. We administered IdU to an adult C57/Bl6 mouse for 7 consecutive days through drinking water and killed it at the end of 7 d of treatment. After rigorous denaturation (100 mM citrate buffer, pH 6.0, boiled for 2.5 min) of the tissue, IdU-labeled cells within the myenteric plexus were found within cross-sections of the ileum that expressed the pan-neuronal marker PGP9.5, and hence were neurons (Fig. 8*A* and Fig. S4 *I* and *J*). Cells within the intestinal crypts were also found to be labeled with IdU (Fig. 8*A*) validating our method.

Nestin-creER^{T2}:tdTomato mice were then given a single dose of tamoxifen, followed a day later by a week-long pulse of IdU and in turn followed by a week-long pulse of a different thymidine analog, CldU, immediately after which the mice were killed. Both IdU and CldU are detected by anti-BrdU antibodies that selectively cross-react to either IdU or CldU (48). If our hypothesis was correct, then during the first week, stem cells should take up IdU, and if they undergo asymmetrical division, then both the differentiated and the daughter stem cells will be labeled with IdU. Subsequent exposure to another label (CldU) will then result in only the proliferating daughter stem cell to carry both (IdU and CldU) labels that will in turn be expressed by their differentiated progeny cells. Fig. 8*B* shows a Nestin-derived (tdTomato^{+}) neuron that stains for both IdU and CldU, suggesting that this particular

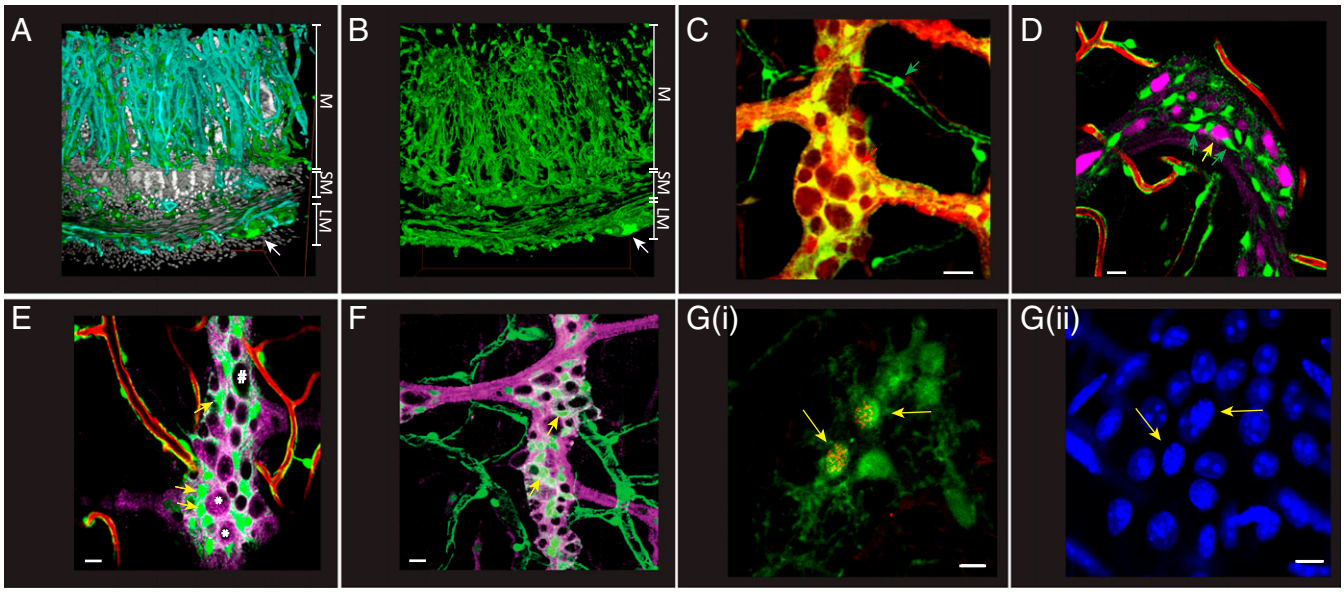

Fig. 5. Distribution of proliferative neural crest-derived putative enteric neural precursor cells in the gut wall. (*A*) A 3D projection image of the gut wall from a Nestin-GFP reporter mouse, where blood vessels are perfusion-painted with DiD (cyan) and nuclei are counterstained with PI (light gray), showing that cells expressing Nestin-GFP (green) form an extensive network that is present in many layers of the gut, ranging from the longitudinal and smooth muscle layer (labeled as LM and SM, respectively) to the mucosa (labeled M). (*B*) A 3D projection of the Nestin-GFP cell network within the gut wall of the adult ileum without vessel and nuclear stain (with longitudinal and smooth muscle layer labeled as LM and SM, respectively, and the mucosa is labeled M). White arrows in *A* and *B* both point toward the location of the myenteric ganglia. Images *A* and *B* captured using a 10× objective lens. (*C*) Image from the myenteric plexus of a Wnt1-cre:tdTomato mouse containing a Nestin-GFP transgene showing that only the Nestin-GFP–expressing cells in the myenteric ganglia (red arrow), and not perivascular cells (green arrow), are of neural crest origin. (*D*) Intraganglionic Nestin-GFP$^+$ cells (green, green arrows) do not express pan-neuronal marker PGP9.5 (magenta, yellow arrow) in a mouse whose vasculature was labeled with DiD (red) indicating that intraganglionic Nestin-GFP expression does not label neurons. (*E*) Only a subpopulation of Nestin-GFP$^+$ cells (green cells) present within the myenteric ganglia and not on the periphery of blood vessels (red) express the low-affinity nerve growth factor receptor p75NTR (magenta), with yellow arrows here labeling some of the double-positive cells. Some p75NTR-expressing cells within the myenteric ganglia do not express Nestin-GFP (*), whereas some other cells express neither Nestin-GFP nor p75NTR (#). (*F*) Similarly, a population of intraganglionic Nestin-GFP$^+$ cells (green cells) express CD49b (magenta) with yellow arrows here labeling some of the double-positive cells. (*G*, *i*) Myenteric ganglia from the ileum of a Nestin-GFP transgenic reporter mouse where Nestin-expressing cells express GFP (green) shows Ki67$^+$ cells (red; yellow arrows) that also express Nestin-GFP; (*ii*) DAPI (blue) labeling of nuclei shows that the Ki67$^+$ Nestin-GFP cells (yellow arrows) show a different staining profile compared with other cells. (Scale bars in *C*–*G*, 10 μm.)

neuron was derived from a Nestin-expressing ENPC that cycled at least twice in the 2 wk after tamoxifen induction to generate a neuron.

As shown in Fig. 8*C*, of all of the HuC/D$^+$ neurons, an average of 11.5% of neurons had no label, and hence were born before the 2-wk experiment; an average of 17% were only labeled with IdU and therefore were born from cells that cycled in the first week; 66% were labeled with both IdU and CldU, and therefore were born from cells that cycled at least twice in 2 wk and 4.75% were labeled with only CldU, suggesting that they were born from cells that cycled in the second week and had either already diluted their IdU label or never had it to begin with. Thus, ∼88% of all myenteric ganglia neurons that were labeled with HuC/D are only 2-wk-old, indicating a high rate of neurogenesis. Despite the evidence of copious neurogenesis, we found as before (Fig. 2*F*), that the numbers of neurons in myenteric ganglia remains constant during this entire time (Fig. 8*D*), consistent with ongoing attrition from apoptosis shown previously.

Targeted Deletion of Phosphatase and Tensin Homolog in Adult ENPCs Reproduces the Phenotype of Some Forms of Chronic Intestinal Pseudo-Obstruction. If enteric neurons are derived from proliferating Nestin$^+$ cells, then changes in their cycling behavior should disrupt ENS morphology and function. We have previously shown that changes in phosphatase and tensin homolog deleted on chromosome 10 (PTEN) signaling in putative adult ENPC in an in vitro model results in increased ENPC proliferation (40). We therefore deleted the PTEN gene in adult Nestin-expressing cells using Nestin-PTEN cKO mice. After tamoxifen induction, small intestinal myenteric ganglia in the Nestin-PTEN cKO mice were larger than those in the Nestin-PTEN WT mice (Fig. 9 *A* and *B*), with a significant increase in both the average numbers of neurons per ganglia ($n = 3$ mice per group, mean ± SE numbers neurons per ganglia: 17.79 ± 1.3 and 41.25 ± 3.4 for PTEN WT and PTEN cKO, respectively, $P = 0.003$) (Fig. 9*C*) and the size of neuronal soma [$n = 3$ mice per group, mean ± SE soma size (measured as Feret diameter): 15.4 ± 0.44 μm and 20.00 ± 0.41 μm for PTEN WT and PTEN cKO, respectively, $P = 0.001$] (Fig. 9*D*). In addition, we found that the whole-gut transit time for PTEN cKO mice was significantly more than PTEN WT animals ($n = 8$ mice per PTEN cKO group and $n = 3$ per PTEN WT group, mean ± SE gastrointestinal transit time of dye: 158.8 ± 20.17 min and 231.7 ± 14.33 min for PTEN WT and PTEN cKO, respectively; Mann–Whitney test: $P = 0.04$) (Fig. 9*E*).

Relationship of ENPC to Glia. Given their expression of S100β, it is conceivable that ENPC are glial cells. To test this hypothesis, we studied the coexpression of Nestin and Sox10. Sox10 is expressed by neurogenic migrating ENPC during embryogenesis and development, but in adults it only marks mature enteric glia (8, 44). For this experiment, we used adult Sox10-H2BVenus mice, in which all myenteric Sox10-expressing cells are labeled with the fluorescent reporter protein Venus (44). When stained for Nestin, myenteric ganglia from these mice showed no detectable overlap between Sox10 and Nestin (Fig. S6*A*). We further tested the expression of conventional glial markers GFAP and S100β in the Nestin-GFP$^+$/p75NTR$^+$ ENPC population in adult mice using FACS analysis. Although Nestin-GFP$^+$ p75NTR$^+$ cells express GFAP and S100β, not all GFAP$^+$ or S100β$^+$ cells expressed either Nestin-GFP or high levels of p75NTR (Fig. S6 *B*–*G*). Thus, expression of

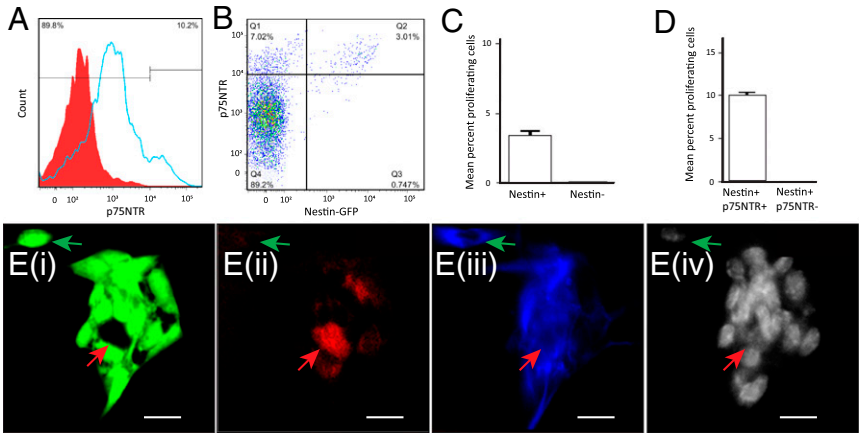

Fig. 6. The ability for in vitro proliferation and neurogenic differentiation is restricted to myenteric cells that coexpress Nestin-GFP and p75NTR. (*A*) p75NTR immunostaining labels most cells positive at varying intensities (blue curve) compared with unstained cells shown here in a red-shaded curve, but only highly labeled cells (10.2% of cells) are deemed positive. These data are used for setting up the flow sorting gates for p75NTR^{+} population. (*B*) Cells flow-sorted for their Nestin-GFP and p75NTR staining according to the gates set in the four quadrants. (*C*) In vitro clonal analyses performed in completely defined medium of flow sorted single cells from the LM-MP layer of a Nestin-GFP reporter mouse shows that only Nestin-GFP expressing cells harbored proliferative potential. (*D*) In vitro clonal analyses performed in completely defined medium of flow sorted single Nestin-GFP–expressing cells stained with antibodies against p75NTR shows that Nestin-GFP and p75NTR coexpressing cells alone have the proliferative potential. (*E*) The clonally derived neurospheres were differentiated in defined culture medium containing Neurobasal medium, B27, BSA, and β-mercaptoethanol, but without growth factors, to generate differentiated cells, some of which showed (*i*) continued expression of Nestin-GFP (green), whereas others gave rise to (*ii*) PGP9.5-expressing neurons (red, red arrow), which did not show Nestin-GFP coexpression, or (*iii*) GFAP-expressing cells (blue) that may show colocalization of Nestin-GFP (green arrow). Nuclei are labeled with DAPI (*iv*), shown here in light-gray color. (Scale bars, 10 μm.)

GFAP or S100β by themselves is not sufficient to identify the adult ENPC. Our results, together with data from other studies (49, 50), suggests that true glia express Sox10, whereas ENPC do not. Adult ENPC are therefore not enteric glia, although they express certain genes also associated with enteric glia.

Discussion

Although neurogenic cells have been shown to exist in adult murine and human gut, the demonstration of their stem-cell like behavior has been mainly restricted to in vitro experiments (7, 12, 13, 22, 40, 51–53). Until now, most studies have suggested that there is no adult enteric neurogenesis in vivo in the healthy gut (7–9, 54). However, in the presence of ongoing neuronal loss and degeneration, as shown in a recent report (27), we do not know how adult myenteric neuronal numbers can be maintained for much of the adult life. Given the conflicting reports on this topic in the literature (5, 6, 26, 55–58), it was first important to rigorously establish and quantify apoptosis in adult enteric neurons. The use of multiple protocols for testing the presence of apoptotic neurons allowed us to confidently prove a high rate of myenteric neuronal apoptosis in the healthy gut. Approximately 11% of myenteric neurons at any one time are labeled by cleaved caspase-3, suggesting that they are fated for programmed cell death. We also found that significantly high (~31%) numbers of labeled neurons were lost in a 7-d period, translating into a 4–5% loss of per day. The fact that approximately half the numbers that are fated for apoptosis (by cleaved caspase-3 labeling) die daily implies that it takes about 2 d for a neuron to die after initiation of apoptosis, which is consistent with what has been previously reported for other kinds of neurons (59). The physiological role of apoptosis was highlighted by the use of a caspase inhibitor, which resulted in an increase in myenteric neuronal counts. Finally, we also show the presence of a robust phagocytic response driven by the abundant numbers of muscularis macrophages, which are known to be associated with myenteric neurons (33), to clear the debris left from the significant numbers of dying neurons.

Together, these results show a high turnover of enteric neurons in the adult gut, which can only be reconciled by invoking ongoing neurogenesis, which in turn necessitates the existence of an ENPC. Previous attempts to define adult ENPC have relied on in vitro demonstration of stem-cell like behavior of cells expressing various markers, such as Sox10, GFAP, p75NTR and CD49b, and Nestin (7–9, 11–18, 20–23). Among these markers, we focused on Nestin because of the existence of transgenic animals expressing the Cre recombinase enzyme under the nestin promoter, allowing us to visualize and isolate these cells, follow their fate in vivo and genetically manipulate the expression of other proteins in them (38, 39, 41, 42). Using Nestin-GFP transgenic reporter mice, we show that cells that coexpress Nestin with the neural crest stem cell marker, p75NTR, do not express neuronal markers and are located within the myenteric ganglia. This is the only cell population that is capable of proliferation and neurogenesis in vitro in defined culture conditions. By following the fate of these cells in adult inducible Nestin-creER^{T2}:tdTomato mice, we found that Nestin-expressing cells gave rise to adult myenteric neurons in the healthy gut, suggesting that these cells are the true ENPC. A previous study has described a putative ENPC in the adult murine colon and suggested proliferation and migration into the myenteric plexus from an extraganglionic location after treatment with a 5HT4 agonist (9). More recently, extraganglionic Schwann cell precursors were observed to generate myenteric neurons in the colon, but not in the small intestine (45). In contrast to these two studies, we show that adult Nestin^{+} precursors for small intestinal myenteric neurons are present inside the myenteric ganglia, suggesting regional differences in enteric neurogenesis.

Our results also suggest that true ENPC are not mature enteric glia, as was previously suggested (60). Although Sox10-expressing cells in the adult myenteric plexus layer retain neurogenic properties in vitro (44), such ability in vivo at steady state remains restricted to embryonic and early postnatal stages (8). Somewhere between the two phases of embryonic ENS "development" and adult ENS "maintenance," there is a switch in ENPC marker profile from Sox10 to Nestin. Indeed, recent work in zebrafish ENS development shows that the neural precursors in the developing gut are also heterogeneous for their Sox10 expression, with neurogenic Sox10^{-} cells present behind the migrating wave front of Sox10^{+} multipotent enteric neural crest precursors (61). Together with our findings, these reports lead to a plausible hypothesis that Sox10^{+} mature glial cells in the adult gut have restricted ability to generate neurons in vivo and only under certain injurious conditions (8), whereas Nestin^{+}/Sox10^{-} precursors are responsible for adult neurogenesis in health.

Definitive proof of the precursor nature of these cells was their ability, under conditions that promoted unchecked proliferation,

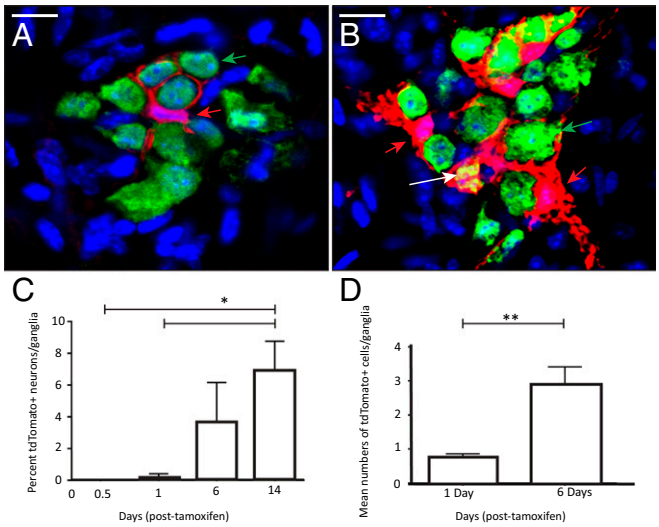

Fig. 7. In vivo neurogenesis from proliferating Nestin-expressing cells within the adult myenteric ganglia. In a Nestin-creER^{T2}:tdTomato mouse induced with tamoxifen at clonal dose, we observe that (*A*) 12 h after tamoxifen induction, tdTomato$^+$ cells in the myenteric ganglia (red; red arrow) do not overlap with the pan-neuronal marker HuC/D (green; green arrow), whereas (*B*) 6 d after the induction, we observe a population of HuC/D$^+$ (green) cells in the myenteric ganglia emerge that express tdTomato (red) and fluoresce yellow (marked here by white arrow). The same ganglia also contain HuC/D-labeled (green) neurons that are not derived from tdTomato-expressing cells (green arrow). tdTomato$^+$ cells that do not express HuC/D also persist in the myenteric ganglia (red arrow). Nuclei in both images are counterstained using DAPI (blue). (Scale bars, 10 μm.) Furthermore, (*C*) compared with 12- and 24-h posttamoxifen induction, we observe an increase in the numbers of tdTomato expressing HuC/D$^+$ neurons at 6 and 14 d (*$P < 0.05$), suggesting continuing derivation of neurons from Nestin-expressing cells. (*D*) tdTomato$^+$ cells within the myenteric ganglia proliferate in vivo, as indicated by their significant increase in numbers 6 d after being labeled at a clonal dose (**$P < 0.001$).

to reproduce the phenotype of certain human diseases. A change in enteric neuronal number is associated with chronic intestinal pseudo-obstruction, a chronic debilitating condition with slow intestinal motility and related complications. Both decreases (hypoganglionisis) and increases (hyperganglionosis) in myenteric neurons have been associated with chronic intestinal pseudo-obstruction. The latter include several human conditions, such as intestinal neuronal dysplasia (IND) or ganglioneuromatosis, which are probably heterogeneous disorders with subsets of patients showing marked reduction in the expression of PTEN (24). Taken together with our previous in vitro results that adult ENPC cycle and generate neurons in a PTEN-dependent manner (40), the present work suggests that adult neurogenesis in vivo may also be controlled by a molecular pathway involving PTEN expression.

We recognize that our findings contradict current dogma in the field, which postulates that populations of adult enteric neurons, once born, remain static until death by disease or senescence. Indeed, previous reports have apparently failed to find evidence of neurogenesis by following the fate of adult Sox10-expressing cells that were assumed to be adult ENPC (8). This discrepancy can now be explained by our demonstration that ENPC do not express Sox10. On the other hand, ENPC do express glial markers like GFAP and others have attempted to use GFAP for fate-mapping experiments in adult neurons, with results that also apparently conflict with ours (7). These investigators used an adult inducible transgenic hGFAP-creER^{T2} mouse bred with a floxed YFP reporter transgenic mouse on a B6 background that was given a long-term exposure to tamoxifen (6–8 mo). However, only 3–5% of GFAP$^+$ cells actually underwent tamoxifen-induced *cre* recombination to become YFP$^+$. Given this reduced rate of transgene expression along with additional problems related to reporter expression with age (62), it is not surprising that these investigators saw a very small proportion of neurons that appeared to be derived from adult GFAP-YFP$^+$ cells. Furthermore, because all of the tamoxifen-induced hGFAP-creER^{T2} mice were killed at the same time of posttamoxifen treatment, Joseph et al. could not observe whether or not this GFAP-derived neuronal population expands with time (7). Nevertheless, the fact that such low numbers of recombinant YFP$^+$ cells were still able to generate a population of neurons at steady state is consistent with our results.

In this report, we also addressed another discrepancy in the literature, namely the inability by Joseph et al. (7) to demonstrate in vivo neurogenesis using BrdU labeling. We next address the issue of why previous reports, using BrdU pulse-chase techniques, failed to demonstrate neurogenesis from cycling precursors

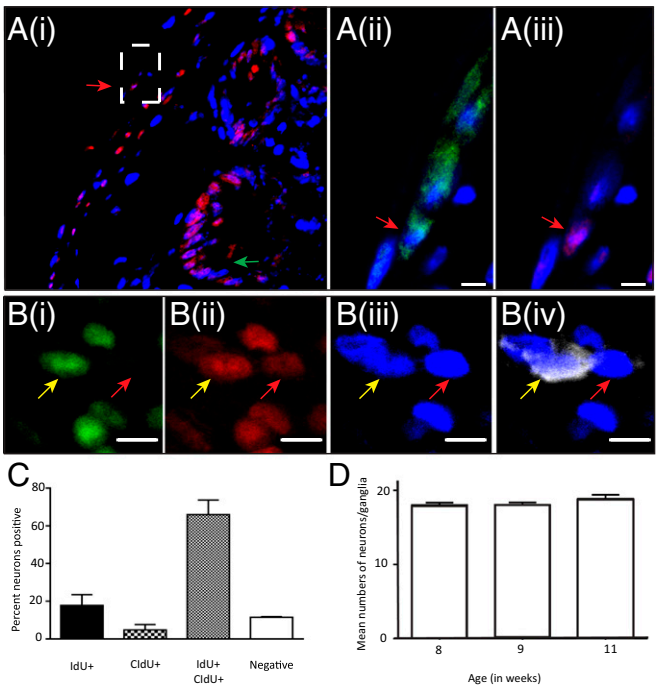

Fig. 8. Label-retaining experiments show rapid and robust myenteric neurogenesis from proliferating Nestin-expressing precursor cells. (*A*, *i*) IdU staining, following 100 mM citrate buffer denaturation of a cross-section (14-μm thick) of ileum from an adult C57BL/6 WT mouse that was dosed with IdU for 7 d and killed immediately after, shows expected positive staining in the intestinal crypt (green arrow) along with staining in the LM-MP layer (red arrow, dashed rectangle magnified in subsequent panels). (*ii*) PGP9.5 immunoreactive neuron (green, red arrow), where nuclei are counterstained with DAPI (blue), (*iii*) is also labeled with specific antibodies against IdU (red), suggesting the presence of newborn neurons derived from precursor cells that cycled during the IdU pulse. (Scale bars, 10 μm.) (*B*, *i*) CldU-labeled (green) and (*ii*) IdU-labeled (red) cells that express (*iii*) HuC/D (blue) and (*iv*) tdTomato (cyan) are neurons (yellow arrow) that are derived from tdTomato$^+$ Nestin-expressing cells that have cycled at least twice, during the IdU as well as CldU pulse to generate neurons. Because of tamoxifen given at a clonal dose, only a subpopulation of precursor cells and their derivative neurons express tdTomato. Same figure and panels shows a neuron (red arrow) derived from a precursor cell that cycled only during IdU pulse where presence of IdU (red) can be detected but no CldU (green) can be detected. (Scale bars, 10 μm.) (*C*) The percentages of neurons that are born with a single label (IdU$^+$ or CldU$^+$), hence derived from precursor cells that cycled only once in either conditions, compared with neurons born with both labels, and hence derived from precursor cells that cycled in both the conditions to generate neurons. This finding suggests that the rate of cycling of the precursor cells is high. We also see a small population of neurons born from precursors that did not cycle during the experiment and hence were either born during the experiment but from cells that cycled just before the experiment or were born before the experiment. (*D*) In healthy adult mice, we observe that the mean numbers of neurons in myenteric ganglia of adult littermates are highly conserved across 21 d of sampling.

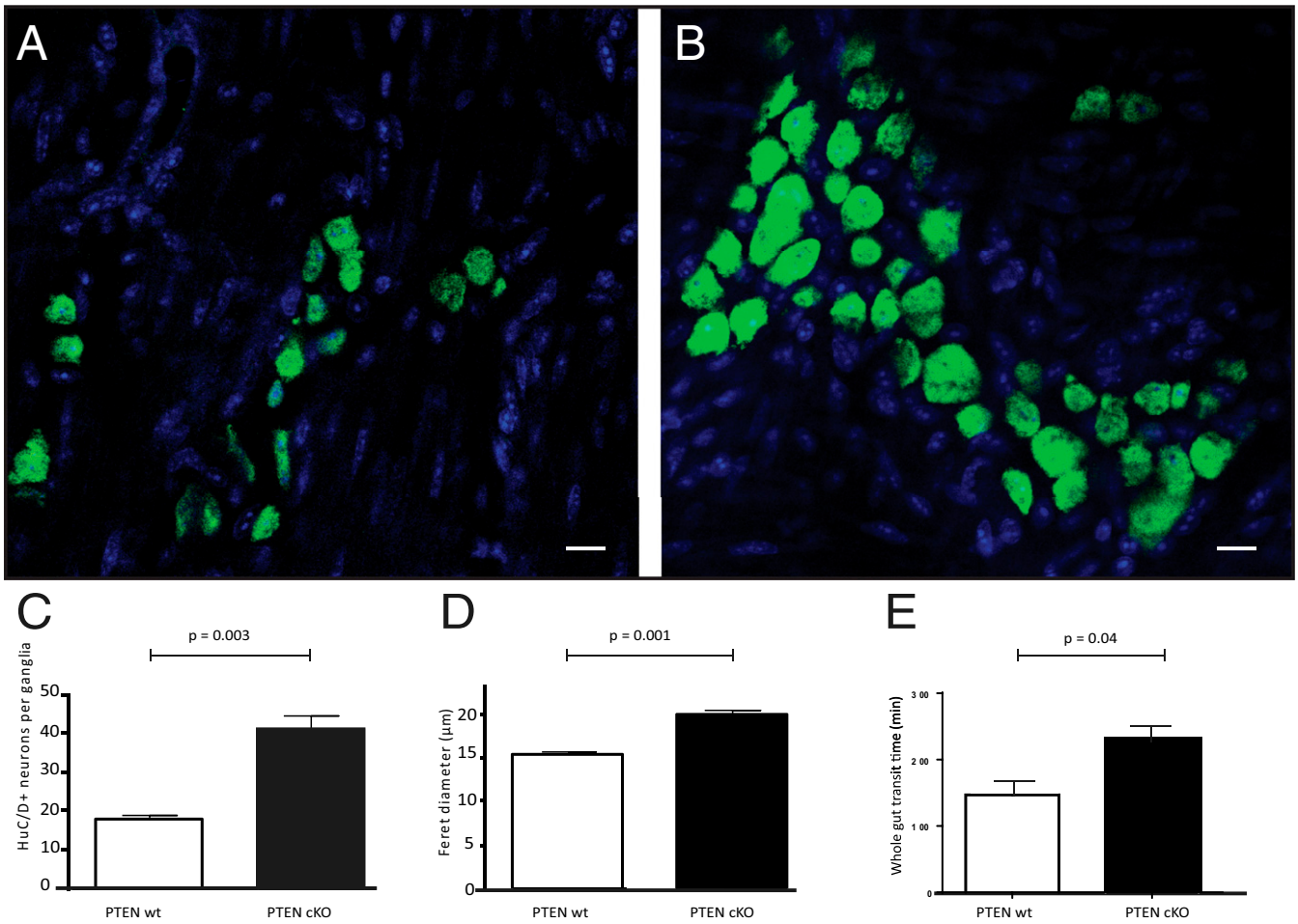

Fig. 9. Knocking out PTEN in adult ENPC significantly increases neuronal numbers and size with a significant increase in whole-gut transit time. (*A* and *B*) Photomicrographs showing HuC/D stained (green) neurons in the myenteric ganglia of Nestin-PTEN WT and Nestin-PTEN cKO mice, respectively, 30 d after induction with tamoxifen. Nuclei are counterstained with DAPI (blue). (Scale bars, 10 μm.) We observe that (*C*) there are significantly more HuC/D$^+$ neurons in the myenteric plexus of the Nestin-PTEN cKO mice compared with their WT control Nestin-PTEN WT mice, and that (*D*) the mean size of neurons (denoted by Feret diameter: diameter of the neuronal cell soma) is significantly higher in Nestin-PTEN cKO mice, than in their WT controls ($P < 0.05$). (*E*) Nestin-PTEN cKO mice 30 d after induction with tamoxifen show a significantly increased whole-gut transit time of carmine red dye compared with age-matched Nestin-PTEN WT mice that were similarly induced with tamoxifen ($P = 0.04$).

(7, 8, 54). We reasoned that if the ENPC population truly has a high turnover rate, decay of label-retention marker to below detection levels could have been a significant confounding factor (63). We therefore designed a labeling and detection protocol for shorter chases and harsher DNA denaturation. Using these techniques for temporally dispersed administration of distinct thymidine analogs, we show that adult enteric neurogenesis results from cycling neural precursors that express Nestin. After 2 wk of treatment with the thymidine analogs, ~88% of all neurons that were labeled with HuC/D showed evidence of label-retention, and hence were newly born. Although this number is very high, it helps explain how myenteric neuronal numbers can be maintained despite very high rates of neuronal apoptosis. When apoptosis was arrested, we saw an ~50% increase in numbers of neurons per ganglia in a week, which reconciles with ~88% of newborn neurons in 2 wk.

The surprisingly high rate of neuronal turnover raises several questions that remain to be answered in future studies. Our results are confined to the small bowel and we do not know whether other regions of the gut express the same paradigm of neurogenesis. Our results with in vivo imaging show a rapidly changing neuronal network, indicating a highly dynamic nervous system that is constantly losing old connections and making new ones. At this time we do not fully understand how functional circuits are built or maintained in the ENS, but a likely explanation for the lack of physiological disruption from this turnover is that it is staggered in time and space, along with the significant redundancy of such circuits within a given region of the gut (64–67).

This rate of turnover in the ENS is either a result of an intrinsically short life of mature neurons or of injury from constant mechanical stress (tensile, compressive, and shear) exerted on the myenteric plexus by virtue of it being sandwiched between the longitudinal and circular muscle (3). In addition, because of its proximity to bowel contents, the ENS is uniquely vulnerable to external threats (4, 68). Nevertheless, a relatively small population of ENPC in the myenteric ganglia appears to be capable of replacing large numbers of dead or dying neurons. As our previous calculations show, adult myenteric neurons die at a rate of a single neuron per ganglia per day, which is not beyond the capacity of a rapidly cycling cell. An alternative mechanism involves a pool of intermediate "transit-amplifying" cells that are fate-committed and cycle to generate large numbers of terminally differentiated cells, as is done by the intestinal stem cells (69). Whether such neurogenic transit-amplifying cells exist in the adult myenteric ganglia is not currently known, and understanding the differentiation pattern of ENPC to form adult neurons would be part of the next steps in understanding the complex biology of the adult ENS.

In conclusion, our study shows evidence of a robust and rapid turnover of adult enteric neurons from identifiable neuronal

precursors that are not mature glial cells (Fig. S7). These findings have considerable scientific and clinical significance. Reliance on this mechanism to maintain neuronal numbers in the presence of ongoing apoptosis may render the ENS at risk from disturbances in this process. For example, a recent study shows that the anticancer chemotherapeutic agent 5-FU, a thymidine synthesis blocker that targets cycling cells, causes a reduction in populations of adult myenteric neurons (70). Similarly, reports of increased apoptosis in myenteric neurons in adult mice with high-fat diet-induced obesity (58) are not always associated with a corresponding loss of myenteric neurons, suggesting active replacement (71). In another case of clinical and physiological relevance, aging is associated with both decreased presence (72) and proliferative potential of ENPC, as well as increased neuronal apoptosis (27), which together could account for the observed reduction in neuronal numbers with age (64). These reports can now be better understood in a construct where the ENS is dynamically maintained by a balance between apoptosis and neurogenesis. Furthermore, as we have shown, targeting genetic mutations in the identified ENPC has the potential for developing novel models of human disease. Therefore, by identifying the participating cells and their molecular profile, our study provides a scientific foundation to study the pathogenesis of disorders of motility, as well as therapeutic targets for the same.

Methods

Animals. All mice used for the experiments were between the ages of 8 and 24 wk and are designated as adult mice. Experimental protocols were approved by Stanford University's Administrative Panel on Laboratory Animal Care, Pennsylvania State's Institutional Animal Care and Use Committee (IACUC), Vanderbilt University's IACUC, Duke University IACUC, as well as by The Johns Hopkins University's Animal Care and Use Committee in accordance with the guidelines provided by the National Institutes of Health. Details of WT and transgenic mice used for the experiments are presented in *SI Methods*.

Protocols for tamoxifen induction; cell culture and transplantation experiments. These methods are expanded in *SI Methods*.

Tissue preparation, cell isolation experiments. Tissue preparation was performed as described before (12, 40), which along with immunohistochemistry (for antibodies see Table S1) and cell isolation protocols are described in *SI Methods*.

Protocols for IdU and CldU labeling, detection, and quantification. Post tamoxifen induction, the mice were given 1 mg/mL of IdU by drinking water for 7 d, after which the IdU-laced drinking water was exchanged with drinking water containing 1 mg/mL of CldU for 7 more days. The mice were then killed, and LM-MP preparations (see below) fixed in freshly made ice cold 4% paraformaldehyde solution. For the whole-mount stainings, we tested denaturation with 10% EDTA (47) at both room temperature and at elevated temperatures (50 °C) for 15 min and found the tissue unresponsive to any immunohistochemistry using either the BrdU antibodies or the anti-HuC/D sera. These experiments with EDTA were followed by testing CldU and HuC/D immunostaining with control tissue (from animals without exposure to CldU) and test tissue (from animals dosed with CldU for 1 wk) that were exposed to 2 N HCl at 50 °C for varying amounts of time (5, 10, and 15 min), and then were immediately washed after thrice with 1× PBS (15 min per wash). The control tissues did not give any reaction to CldU antibodies, whereas the test tissues saw an increase in the numbers of cells around and within the myenteric ganglia with exposure to the denaturing agent (Fig. S3 *B* and *C*). Exposure to 2 N HCl at elevated temperatures beyond 15-min hampered tissue integrity and created impediment to immunostaining and visualization. This standardized protocol was used for immunostaining the IdU/CldU-stained tissues. IdU/CldU was then labeled with anti-BrdU antibodies that selectively cross-label either IdU or CldU [B44 antibody selectively cross-reacts with IdU (BD Biosciences) and Bu1/75 selectively cross-reacts with CldU (Novus Biologicals)] (48) and counterstained with anti-mouse 546 antibody (against B44 IdU antibody) and anti-rat 488 antibody (against Bu1/75 CldU antibody) (Invitrogen). The acid treatment destroys all native fluorescence and changes cell structure, so tdTomato expression needs to be revealed by immunofluorescence. Hence, the tissues were stained with anti-RFP antibody (Rockland) in addition to HuC/D antisera (ANNA1). The anti-RFP antibody was counterstained with anti-rabbit 647 antibody (Invitrogen) and the HuC/D antisera was counterstained with anti-human Brilliant Violet 421 antibody (Biolegend). The tissues were mounted with mounting medium without DAPI (Vector Labs). Control tissues of LM-MP that were never dosed with IdU/CldU were similarly denatured and stained. Slight staining in the nucleoli was regarded as a denaturation-based autofluorescence, but copious staining in the whole nucleus in a HuC/D-labeled cell was deemed as a positively labeled neuron. As a technical limitation of performing acid treatment, a prerequisite of staining for label-retention, on whole mounts of intestines to visualize and enumerate enteric neurons, the size and shape of cells is changed and not all neurons are labeled with HuC/D. Hence, for the quantification, only neurons labeled convincingly with HuC/D antisera are counted, and hence represent a subpopulation of all myenteric neurons.

Detecting apoptosis in enteric neurons. Fixed LM-MP tissues from an adult C57BL/6 mouse were stained for cleaved caspase-3, a marker for apoptosis using the antibody Asp175 (Cell Signaling). The tissues were counterstained with DAPI, overlaid with Vectashield mounting medium (Vector Labs), coverslipped, and imaged using a Leica 510 confocal microscope. The images then were analyzed using Fiji software (fiji.sc). A HuC/D-labeled cell in the myenteric ganglia with strong immunostaining for cleaved caspase-3 in the perinuclear space (26, 56, 73) was counted as an apoptotic neuron. Other methods for detecting apoptotic neurons are presented in *SI Methods*. Small intestinal ganglia were demarcated as previously described (27) and their neuronal density was represented as neurons/ganglia as previously reported (74).

Imaging experiments. Protocols for fixed tissue confocal imaging, live animal confocal imaging, as well as two-photon imaging experiments are described in *SI Methods*.

Statistics. All the quantified data is presented in Tables S2–S8. Data are expressed as the mean ± SE for every graphical representation. Statistical analysis was performed with the aid of Graphpad Prism. A Mann–Whitney test and and Kruskall–Wallis test were used to compare means for statistically significant difference between two and three groups, respectively. Statistical significance (*) was assumed if $P < 0.05$.

ACKNOWLEDGMENTS. We thank Prof. Jeremy Nathans (The Johns Hopkins University) and Prof. Ben Barres (Stanford University) for their scientific advice and critical comments; Dr. Charles Chan (Stanford University) for help with standardizing tissue digestion protocols; Dr. Martin Bigos for help with standardizing flow-sorting protocols; and Mithra Kumar (The Johns Hopkins University) for help with mouse colony management. FACS sorting was done with the help of the Beckman Flow Sorting Core at Stanford University, and FACS analysis was performed at the Ross Flow Sorting Core at The Johns Hopkins University and at the Flow Cytometry Core Facility in the Department of Comparative Medicine at the Pennsylvania State University. Confocal microscopy was performed using the Ross Confocal Microscopy Core, the MicFac at The Johns Hopkins University, the NIS microscopy facility at Stanford University, Sravya Kurapati (Pennsylvania State Biomedical Sciences PhD Program), and Thomas Abraham with the Microscopy Imaging Facility (Pennsylvania State University College of Medicine). This work was supported by National Institute of Diabetes and Digestive and Kidney Diseases Grant R01DK080920 (to P.J.P.); Grant P30 DK089502 (Conte Digestive Diseases Basic and Translational Research Core Center at the Johns Hopkins University); NIH Grants OT2-OD023849 and R01GM114254 (to X.S.); Defense Advanced Research Planning Agency Grant N660015-2-4059 (to X.S.); NIH Grants R01DE022750 and R01GM087369 (to X.D.); a Johns Hopkins University Brain Science Institute grant and the Howard Hughes Medical Institute (to X.D.); an innovation award from the Kenneth Rainin Foundation (to M.B.); National Institute of Allergy and Infectious Diseases Grant R21 AI126351 01 (to M.B.); and March of Dimes Grant 1FY-12-450) (to E.M.S.-S.).

1. Furness JB (2012) The enteric nervous system and neurogastroenterology. *Nat Rev Gastroenterol Hepatol* 9:286–294.
2. Ouyang A, Locke GR, 3rd (2007) Overview of neurogastroenterology-gastrointestinal motility and functional GI disorders: Classification, prevalence, and epidemiology. *Gastroenterol Clin North Am* 36:485–498, vii.
3. Mazzuoli-Weber G, Schemann M (2015) Mechanosensitivity in the enteric nervous system. *Front Cell Neurosci* 9:408.
4. Anitha M, et al. (2016) Intestinal dysbiosis contributes to the delayed gastrointestinal transit in high-fat diet fed mice. *Cell Mol Gastroenterol Hepatol* 2:328–339.
5. Gabella G (1971) Neuron size and number in the myenteric plexus of the newborn and adult rat. *J Anat* 109:81–95.
6. Thrasivoulou C, et al. (2006) Reactive oxygen species, dietary restriction and neurotrophic factors in age-related loss of myenteric neurons. *Aging Cell* 5:247–257.
7. Joseph NM, et al. (2011) Enteric glia are multipotent in culture but primarily form glia in the adult rodent gut. *J Clin Invest* 121:3398–3411.
8. Laranjeira C, et al. (2011) Glial cells in the mouse enteric nervous system can undergo neurogenesis in response to injury. *J Clin Invest* 121:3412–3424.
9. Liu MT, Kuan YH, Wang J, Hen R, Gershon MD (2009) 5-HT4 receptor-mediated neuroprotection and neurogenesis in the enteric nervous system of adult mice. *J Neurosci* 29:9683–9699.
10. Pham TD, Gershon MD, Rothman TP (1991) Time of origin of neurons in the murine enteric nervous system: Sequence in relation to phenotype. *J Comp Neurol* 314:789–798.

11. Almond S, Lindley RM, Kenny SE, Connell MG, Edgar DH (2007) Characterisation and transplantation of enteric nervous system progenitor cells. *Gut* 56:489–496.
12. Becker L, Kulkarni S, Tiwari G, Micci MA, Pasricha PJ (2012) Divergent fate and origin of neurosphere-like bodies from different layers of the gut. *Am J Physiol Gastrointest Liver Physiol* 302:G958–G965.
13. Bixby S, Kruger GM, Mosher JT, Joseph NM, Morrison SJ (2002) Cell-intrinsic differences between stem cells from different regions of the peripheral nervous system regulate the generation of neural diversity. *Neuron* 35:643–656.
14. Bondurand N, Natarajan D, Thapar N, Atkins C, Pachnis V (2003) Neuron and glia generating progenitors of the mammalian enteric nervous system isolated from foetal and postnatal gut cultures. *Development* 130:6387–6400.
15. Heanue TA, Pachnis V (2010) Prospective identification and isolation of enteric nervous system progenitors using SOX2. *Stem Cells* 29:128–40.
16. Lo L, Anderson DJ (1995) Postmigratory neural crest cells expressing c-RET display restricted developmental and proliferative capacities. *Neuron* 15:527–539.
17. Metzger M (2010) Neurogenesis in the enteric nervous system. *Arch Ital Biol* 148: 73–83.
18. Metzger M, et al. (2009) Expansion and differentiation of neural progenitors derived from the human adult enteric nervous system. *Gastroenterology* 137: 2063–2073 e2064.
19. Metzger M, Caldwell C, Barlow AJ, Burns AJ, Thapar N (2009) Enteric nervous system stem cells derived from human gut mucosa for the treatment of aganglionic gut disorders. *Gastroenterology* 136:2214–2225.e1-3.
20. Natarajan D, Grigoriou M, Marcos-Gutierrez CV, Atkins C, Pachnis V (1999) Multipotential progenitors of the mammalian enteric nervous system capable of colonising aganglionic bowel in organ culture. *Development* 126:157–168.
21. Rauch U, Hänsgen A, Hagl C, Holland-Cunz S, Schäfer KH (2006) Isolation and cultivation of neuronal precursor cells from the developing human enteric nervous system as a tool for cell therapy in dysganglionosis. *Int J Colorectal Dis* 21:554–559.
22. Suárez-Rodríguez R, Belkind-Gerson J (2004) Cultured nestin-positive cells from postnatal mouse small bowel differentiate ex vivo into neurons, glia, and smooth muscle. *Stem Cells* 22:1373–1385.
23. Schäfer KH, Hagl CI, Rauch U (2003) Differentiation of neurospheres from the enteric nervous system. *Pediatr Surg Int* 19:340–344.
24. Puig I, et al. (2009) Deletion of Pten in the mouse enteric nervous system induces ganglioneuromatosis and mimics intestinal pseudoobstruction. *J Clin Invest* 119: 3586–3596.
25. Sanno H, et al. (2010) Control of postnatal apoptosis in the neocortex by RhoA-subfamily GTPases determines neuronal density. *J Neurosci* 30:4221–4231.
26. Nezami BG, et al. (2014) MicroRNA 375 mediates palmitate-induced enteric neuronal damage and high-fat diet-induced delayed intestinal transit in mice. *Gastroenterology* 146:473–483 e473.
27. Becker L, et al. (2017) Age-dependent shift in macrophage polarisation causes inflammation-mediated degeneration of enteric nervous system. *Gut*, 10.1136/gutjnl-2016-312940.
28. Hristov G, et al. (2014) SHOX triggers the lysosomal pathway of apoptosis via oxidative stress. *Hum Mol Genet* 23:1619–1630.
29. Hussain ST, Attilo A, Bigotte L, Cesarini K, Olsson Y (1985) Cytofluorescence localization of propidium iodide injected intravenously into the nervous system of the mouse. *Acta Neuropathol* 66:62–67.
30. Unal Cevik I, Dalkara T (2003) Intravenously administered propidium iodide labels necrotic cells in the intact mouse brain after injury. *Cell Death Differ* 10:928–929.
31. Brana C, Benham C, Sundstrom L (2002) A method for characterising cell death in vitro by combining propidium iodide staining with immunohistochemistry. *Brain Res Brain Res Protoc* 10:109–114.
32. Rakhilin N, et al. (2016) Simultaneous optical and electrical in vivo analysis of the enteric nervous system. *Nat Commun* 7:11800.
33. Margolis KG, Gershon MD, Bogunovic M (2016) Cellular organization of neuroimmune interactions in the gastrointestinal tract. *Trends Immunol* 37:487–501.
34. Muller PA, et al. (2014) Crosstalk between muscularis macrophages and enteric neurons regulates gastrointestinal motility. *Cell* 158:300–313.
35. Gautron L, et al. (2013) Neuronal and nonneuronal cholinergic structures in the mouse gastrointestinal tract and spleen. *J Comp Neurol* 521:3741–3767.
36. Heng TS, Painter MW; Immunological Genome Project Consortium (2008) The Immunological Genome Project: Networks of gene expression in immune cells. *Nat Immunol* 9:1091–1094.
37. Steinert PM, et al. (1999) A high molecular weight intermediate filament-associated protein in BHK-21 cells is Nestin, a type VI intermediate filament protein. Limited coassembly in vitro to form heteropolymers with type III vimentin and type IV alpha-internexin. *J Biol Chem* 274:9881–9890.
38. Mignone JL, et al. (2007) Neural potential of a stem cell population in the hair follicle. *Cell Cycle* 6:2161–2170.
39. Mignone JL, Kukekov V, Chiang AS, Steindler D, Enikolopov G (2004) Neural stem and progenitor cells in nestin-GFP transgenic mice. *J Comp Neurol* 469:311–324.
40. Becker L, Peterson J, Kulkarni S, Pasricha PJ (2013) Ex vivo neurogenesis within enteric ganglia occurs in a PTEN dependent manner. *PLoS One* 8:e59452.
41. Birbrair A, Wang ZM, Messi ML, Enikolopov GN, Delbono O (2011) Nestin-GFP transgene reveals neural precursor cells in adult skeletal muscle. *PLoS One* 6:e16816.
42. Bonaguidi MA, et al. (2011) In vivo clonal analysis reveals self-renewing and multipotent adult neural stem cell characteristics. *Cell* 145:1142–1155.
43. Fu YY, Peng SJ, Lin HY, Pasricha PJ, Tang SC (2013) 3-D imaging and illustration of mouse intestinal neurovascular complex. *Am J Physiol Gastrointest Liver Physiol* 304: G1–G11.
44. Corpening JC, et al. (2011) Isolation and live imaging of enteric progenitors based on Sox10-Histone2BVenus transgene expression. *Genesis* 49:599–618.
45. Uesaka T, Nagashimada M, Enomoto H (2015) Neuronal differentiation in Schwann cell lineage underlies postnatal neurogenesis in the enteric nervous system. *J Neurosci* 35:9879–9888.
46. Wilm B, Ipenberg A, Hastie ND, Burch JB, Bader DM (2005) The serosal mesothelium is a major source of smooth muscle cells of the gut vasculature. *Development* 132: 5317–5328.
47. Shimada A, Shibata T, Komatsu K, Nifuji A (2008) Improved methods for immunohistochemical detection of BrdU in hard tissue. *J Immunol Methods* 339:11–16.
48. Kimoto M, Yura Y, Kishino M, Toyosawa S, Ogawa Y (2008) Label-retaining cells in the rat submandibular gland. *J Histochem Cytochem* 56:15–24.
49. Boesmans W, Lasrado R, Vanden Berghe P, Pachnis V (2015) Heterogeneity and phenotypic plasticity of glial cells in the mammalian enteric nervous system. *Glia* 63: 229–241.
50. Rao M, et al. (2015) Enteric glia express proteolipid protein 1 and are a transcriptionally unique population of glia in the mammalian nervous system. *Glia* 63: 2040–2057.
51. Azan G, Low WC, Wendelschafer-Crabb G, Ikramuddin S, Kennedy WR (2011) Evidence for neural progenitor cells in the human adult enteric nervous system. *Cell Tissue Res* 344:217–225.
52. Lindley RM, et al. (2008) Human and mouse enteric nervous system neurosphere transplants regulate the function of aganglionic embryonic distal colon. *Gastroenterology* 135:205–216.e6.
53. Hotta R, et al. (2013) Transplanted progenitors generate functional enteric neurons in the postnatal colon. *J Clin Invest* 123:1182–1191.
54. Belkind-Gerson J, et al. (2015) Colitis induces enteric neurogenesis through a 5-HT4-dependent mechanism. *Inflamm Bowel Dis* 21:870–878.
55. Cook RD, Burnstock G (1976) The altrastructure of Auerbach's plexus in the guinea-pig. I. Neuronal elements. *J Neurocytol* 5:171–194.
56. Anitha M, et al. (2006) GDNF rescues hyperglycemia-induced diabetic enteric neuropathy through activation of the PI3K/Akt pathway. *J Clin Invest* 116:344–356.
57. Gianino S, Grider JR, Cresswell J, Enomoto H, Heuckeroth RO (2003) GDNF availability determines enteric neuron number by controlling precursor proliferation. *Development* 130:2187–2198.
58. Stenkamp-Strahm CM, Kappmeyer AJ, Schmalz JT, Gericke M, Balemba O (2013) High-fat diet ingestion correlates with neuropathy in the duodenum myenteric plexus of obese mice with symptoms of type 2 diabetes. *Cell Tissue Res* 354:381–394.
59. Kristiansen M, Ham J (2014) Programmed cell death during neuronal development: The sympathetic neuron model. *Cell Death Differ* 21:1025–1035.
60. Gershon MD (2011) Behind an enteric neuron there may lie a glial cell. *J Clin Invest* 121:3386–3389.
61. Taylor CR, Montagne WA, Eisen JS, Ganz J (2016) Molecular fingerprinting delineates progenitor populations in the developing zebrafish enteric nervous system. *Dev Dyn* 245:1081–1096.
62. Bai X, et al. (2013) Genetic background affects human glial fibrillary acidic protein promoter activity. *PLoS One* 8:e66873.
63. Mandyam CD, Harburg GC, Eisch AJ (2007) Determination of key aspects of precursor cell proliferation, cell cycle length and kinetics in the adult mouse subgranular zone. *Neuroscience* 146:108–122.
64. Gabella G (1989) Fall in the number of myenteric neurons in aging guinea pigs. *Gastroenterology* 96:1487–1493.
65. Garcia SB, et al. (2002) No reduction with ageing of the number of myenteric neurons in benzalkonium chloride treated rats. *Neurosci Lett* 331:66–68.
66. Spencer NJ (2016) Motility patterns in mouse colon: Gastrointestinal dysfunction induced by anticancer chemotherapy. *Neurogastroenterol Motil* 28:1759–1764.
67. Ro S, Hwang SJ, Muto M, Jewett WK, Spencer NJ (2006) Anatomic modifications in the enteric nervous system of piebald mice and physiological consequences to colonic motor activity. *Am J Physiol Gastrointest Liver Physiol* 290:G710–G718.
68. Kabouridis PS, et al. (2015) Microbiota controls the homeostasis of glial cells in the gut lamina propria. *Neuron* 85:289–295.
69. Crosnier C, Stamataki D, Lewis J (2006) Organizing cell renewal in the intestine: Stem cells, signals and combinatorial control. *Nat Rev Genet* 7:349–359.
70. McQuade RM, et al. (2016) Gastrointestinal dysfunction and enteric neurotoxicity following treatment with anticancer chemotherapeutic agent 5-fluorouracil. *Neurogastroenterol Motil* 28:1861–1875.
71. Soares A, Beraldi EJ, Ferreira PE, Bazotte RB, Buttow NC (2015) Intestinal and neuronal myenteric adaptations in the small intestine induced by a high-fat diet in mice. *BMC Gastroenterol* 15:3.
72. Molofsky AV, et al. (2006) Increasing p16INK4a expression decreases forebrain progenitors and neurogenesis during ageing. *Nature* 443:448–452.
73. Gown AM, Willingham MC (2002) Improved detection of apoptotic cells in archival paraffin sections: Immunohistochemistry using antibodies to cleaved caspase 3. *J Histochem Cytochem* 50:449–454.
74. Shirasawa S, et al. (1997) Enx (Hox11L1)-deficient mice develop myenteric neuronal hyperplasia and megacolon. *Nat Med* 3:646–650.
75. Kuo YM, et al. (2010) Extensive enteric nervous system abnormalities in mice transgenic for artificial chromosomes containing Parkinson disease-associated alpha-synuclein gene mutations precede central nervous system changes. *Hum Mol Genet* 19:1633–1650.